Interfacial magnetization in exchange-coupled Fe/Cr/Fe structures investigated by second harmonic generation

A. A. Rzhevsky*
Institut für Festkörperforschung, Forschungzentrum Jülich GmbH, D-52425 Jülich, Germany
and Ioffe Physical Technical Institute, Russian Academy of Sciences, 194021 St. Petersburg, Russia

B. B. Krichevtsov
Ioffe Physical Technical Institute, Russian Academy of Sciences, 194021 St. Petersburg, Russia

D. E. Bürgler and C. M. Schneider
Institut für Festkörperforschung, Forschungzentrum Jülich GmbH, D-52425 Jülich, Germany
(Received 14 September 2006; revised manuscript received 21 December 2006; published 16 April 2007)

We have studied the magnetic field dependences of magnetic optical second harmonic generation (SHG) in MBE-grown Fe/Cr/Fe/Ag/GaAs(100) heterostructures displaying both bilinear and biquadratic interlayer exchange coupling. The magnetic field **H** was applied in the (100) surface plane along both easy ([001]) and hard ([110]) axes of the in-plane fourfold magnetic anisotropy. The SHG has been measured in reflection at near normal incidence for different polarization combinations (pp,ps,ss,sp) of the fundamental and second harmonic light in longitudinal and transversal geometries. The magnetic field variation of the SHG signal clearly reflects the field-induced transformations of the magnetic state at the interfaces in the trilayer. It strongly depends on the configuration of light polarization, experimental geometry (longitudinal or transversal), and orientation of the magnetic field **H** relative to the crystal axes. In contrast to linear magneto-optical Kerr effect, which is odd in magnetic field, magnetic SHG is either even in **H** or does not display a definite parity at all, depending on the polarization configuration. We interpret the data based on a model accounting for nonmagnetic and magnetic contributions to SHG from the surface and interfaces described by C_{4v} point symmetry. Taking into account the changes of the mutual orientation of interfacial magnetizations allows us to describe the general features of the measured field dependences of SHG.

DOI: 10.1103/PhysRevB.75.144416 PACS number(s): 75.70.Cn, 75.30.Et, 78.20.Ls, 42.65.Ky

I. INTRODUCTION

Since its discovery in 1986 (Ref. 1) the coupling of thin magnetic layers (e.g., Fe, Co, Ni) separated by nonferromagnetic interlayers (e.g., Cr, Au) has been a subject of intensive studies. A compilation of the main results up to now can be found in a number of comprehensive reviews.[2–4] It was established, for example, that the parameters defining the actual magnetic state of the coupled system such as the interlayer exchange coupling strength, the saturation magnetizations of the layers, as well as the magnetic anisotropy can vary in wide limits and are governed by an appropriate choice of growth conditions. In particular, the strength of the bilinear exchange interaction J_1 ($E_{bl}=-J_1\hat{\mathbf{M}}_1\hat{\mathbf{M}}_2$, where $\hat{\mathbf{M}}_i$ is a unit vector along the magnetization direction of layer i, $\mathbf{M}_i$) can be positive or negative depending on the thickness of the intermediate layer. In the former case it results in ferromagnetic ($\mathbf{M}_1\uparrow\uparrow\mathbf{M}_2$) and in the latter in an antiferromagnetic alignment ($\mathbf{M}_1\uparrow\downarrow\mathbf{M}_2$) of the magnetization directions of the magnetic layers. At the same time the biquadratic exchange coupling $E_{\mathrm{bq}}=-J_2(\hat{\mathbf{M}}_1\hat{\mathbf{M}}_2)^2$ stimulates an orthogonal orientation of the magnetizations ($\mathbf{M}_1\perp\mathbf{M}_2$) for dominant J_2 and $J_2<0$. The interplay between the two interaction parameters J_1 and J_2 causes the system to display a rich variety of different magnetic configurations (collinear ferromagnetic or antiferromagnetic, orthogonal, canted) depending on the applied field **H**. The stabilization of different magnetic configurations or "phases," which can be switched by relatively weak fields and which are often combined with large magnetoresistance effects [giant magnetoresistance (GMR)],[5,6] make exchange-coupled structures major building blocks for practical applications.

At present the bilinear exchange coupling is well described by theoretical models based on the Ruderman-Kittel-Kasuya-Yosida picture.[4,7–9] At the same time the sources of biquadratic coupling are not completely clear at the moment and different models accounting for various intrinsic or extrinsic factors have been proposed.[10–12] Among these the interface microstructure and magnetic properties at the interface are believed to play a major role in the appearance of the biquadratic coupling.[13]

It is worth noting that up to now the static and dynamic magnetic properties of exchange coupled structures have been mainly studied by methods accessing bulk magnetic properties of the structures such as magneto-optical Kerr effect (MOKE), ferromagnetic resonance, and Brillouin light scattering. These methods allow one to determine bilinear and biquadratic coupling strengths, their variation with interlayer thickness as well as with the type and orientation of the substrate, etc. Some surface-specific approaches such as direct and inverse photoemission and spectroscopy have been used to elucidate the relation between interlayer coupling and quantum-well states in the interlayer.[14–16] X-ray magneto-optical techniques have been applied to study the magnetization distributions in multilayer structures.[17–19] All

of these approaches do not directly provide information about the magnetic state and the behavior of the magnetization immediately at the interfaces. In order to distinguish between volume and interfacial contributions in the exchange coupling mechanisms, specific interface sensitive techniques are required.

In this work the method of magnetic field-induced second harmonic generation (MSHG) is used to study the interfacial magnetization behavior in Fe/Cr/Fe exchange-coupled structures. Since the theoretical predictions in the 1980's[20–23] and subsequent first experimental observations[24–27] the method has been widely used and proved to be a highly sensitive tool to investigate surface and interfacial magnetic properties of thin films and multilayers.[28–32]

The first theoretical activities[22,23] were devoted to the treatment of MSHG (or nonlinear Kerr effect) from infinitely thin magnetic layers, where the electro-dipole SHG appears due to the breaking of the inversion symmetry at the surface or interface. The phenomenological model describing MSHG in magnetic multilayers formed by sequence of magnetic and nonmagnetic centrosymmetric thin films was elaborated in Refs. 33–35. The theory of SHG in metallic sandwich structures of 3*d* metals covered by noble metals was developed to explain the appearance of SHG intensity oscillations due to quantum well states.[36,37] In Ref. 38 the problem of boundary conditions of linear and nonlinear magneto-optical phenomena in multilayers is considered and expressions describing the linear Kerr effect and azimuthal dependences of MSHG for different interface point symmetries and experimental geometries are obtained. A theory of MSHG from arbitrary multilayer systems based on a consideration of the radiation from point dipoles and accounting for spatial derivatives of the nonlinear susceptibility tensors was developed in Ref. 39. The theory was capable to explain a number of experimental results, such as dependence of MSHG on the angle of incidence, and was able to describe MSHG from systems containing buried ferromagnetic layers with small periodic magnetic domains.

Until recently, the experimental investigations of MSHG were mostly focused on probing surfaces or buried interfaces of single or sandwiched magnetic layers.[30,40] At present, large interest has also emerged in the investigation of exchange-coupled as well as exchange-biased multilayer systems. However, only a few experiments devoted to this topic have been performed so far. In particular, the exchange-coupled bilayer system $Fe_{96}Si_4/Dy_{30}Fe_{58}Co_{12}$ characterized by competing magnetic anisotropies and CoO/Co/NiO/Fe-Ni/Cu tunnel junctions displaying nearly perpendicular interlayer coupling were investigated with MSHG in Refs. 32 and 41. The possibility to separate contributions from different interfaces in the total MSHG signal was shown. According to the predictions, this separation mainly profits from the discontinuity of the electric field profile of the incident radiation through the multilayer structure. The field dependences of MSHG in sandwiched Cu/Ni/Cu(100) and exchange-coupled Ni/Cu/Ni/Cu(001) structures composed of ultrathin ($\approx$6 ML) magnetic layers were investigated in Ref. 42. In this work the antiferromagnetic interlayer exchange coupling in the Ni/Cu/Ni trilayer was observed by means of MSHG due to the presence of localized quantum well states (QWSs) in the Cu spacer. The relation of reversible and irreversible uncompensated spins at the interfaces of FeMn/FeNi bilayers with exchange bias was also studied by MSHG.[43] In Refs. 44 and 45 the method of MSHG has successfully been applied to study exchange bias in CoO/Cu/Fe multilayers. The role of uncompensated spins at the interface in the exchange-bias structure was directly demonstrated.

Fe/Cr/Fe structures have been intensively studied over twenty years by different methods and can thus be considered as model systems not only for interlayer exchange coupling, but also for probing different aspects of the interfacial magnetism in such systems. Among these magnetic order and magnetic moment at the interface, proximity effects, the influence of interface roughness on biquadratic coupling and spin density wave formation are very interesting. The most recent results concerning bulk magnetic properties as well as interface probing of these structures can be found in Refs. 46–52. To the best of our knowledge, the investigation of MSHG in Fe/Cr/Fe systems displaying both bilinear and biquadratic interlayer exchange coupling has not been performed. Therefore, the goal of this work is to establish the connection between changes of the magnetic state at the interfaces in an applied magnetic field and changes of the MSHG observed in different experimental geometries. Establishing and understanding such a link are necessary steps for advancing studies of the interfacial magnetism in structures of this type.

In our studies we have chosen the thickness of the Cr interlayer such as to establish an antiferromagnetic coupling between the Fe layers of the Fe/Cr/Fe structures ($t_{Cr} \approx 10$ Å).[13] The structures have been grown on GaAs(100) by molecular beam epitaxy (MBE) providing a high crystalline quality of the layers and interfaces. The magnetic anisotropy in the sample plane of these structures is fourfold (biaxial) with the angle between two equivalent easy $\mathbf{e}_1$ and $\mathbf{e}_2$ (or hard $\mathbf{h}_1$ and $\mathbf{h}_2$) axes being 90°. The angle between corresponding easy and hard axes is 45°. That gave us the possibility to carry out measurements in longitudinal and transverse geometries by changing only the direction of the magnetic field by 90° while maintaining the orientation of the sample. In both geometries the magnetic field was directed either along an easy or hard axis. The choice of the structures was also determined by the fact that the component of SHG, which is linear in $\mathbf{M}$ is large, manifesting itself in a strong magnetic contrast.[53,54]

The analysis of the MSHG field dependences measured in the Fe/Cr/Fe structures is conducted on the basis of an effective susceptibility model discussed in the Sec. IV. For the modeling of the data we used the results of previous theoretical treatments,[32,38,39,55,56] taking into account that the angle of incidence θ in our measurements was close to normal incidence ($\theta \approx 5°$). This allowed us to simplify expressions and to link the values of MSHG in different polarization and magnetic field configurations to certain components of the magnetization vector. Using the geometry with small angles of incidence yields a mechanism to efficiently reduce the nonmagnetic contributions to SHG. Furthermore, this geometry also eliminates the problem of a discontinuity of the normal components of the electric field at the interfaces, i.e., the problem of boundary conditions.[38]

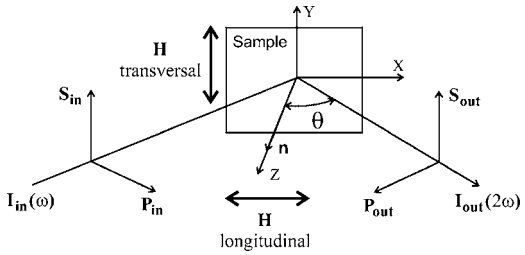

FIG. 1. Geometry of the SHG measurements.

In order to check the validity of this model we also used it to describe the MSHG field dependences measured along with conventional MOKE on more simple Cr/Fe-wedge structures containing only one Fe layer of variable thickness. These measurements allowed us to assess the contribution of the bottom interface to the total MSHG signal in Fe/Cr/Fe structures as well as to estimate the values of effective susceptibilities.

The paper is organized as follows. In Sec. II experimental details of the SHG measurements and sample preparation are given. In Sec. III the results of the SHG field dependence measurements at different orientations of magnetic field and input-output polarization combinations of the light are presented. In Sec. IV the analysis and modeling of the field dependences is conducted based on expressions for SHG from surfaces and interfaces described by C_{4v} point symmetry and accounting for mutual changes in orientations of the magnetizations in the applied magnetic field. In Sec. V the limitations of the model are discussed. In Sec. VI, finally, the main results of the work are summarized.

II. EXPERIMENT

The geometry of the experiment is schematically shown in Fig. 1. The exciting light pulses at $\lambda=800$ nm ($E_{\mathrm{ph}}=\hbar\omega=1.55$ eV) and duration of 200 fs were generated by a Ti:sapphire regenerative amplifier with 1 kHz repetition rate and 1 mJ pulse power. After attenuation down to 15 μJ the pulses were focused into a spot of 0.6 mm diameter on the sample surface. The average power incident on the sample was about 15 mW. The SHG was measured in reflection at $\lambda=400$ nm ($E_{\mathrm{ph}}=2\hbar\omega=3.1$ eV). The fundamental light at $\lambda=800$ nm was rejected by placing a blue filter (BG-39) into the reflected beam. The SHG signal was recorded using a photomultiplier and photon counting technique. The counting time of each experimental point was 10–20 s. A magnetic field up to 3 kOe was applied parallel to the sample surface either in the plane of the incident light (longitudinal geometry) or perpendicular to it (transversal geometry). The angle of incidence was ($\theta\approx 5°$). The polarization of the fundamental and frequency-doubled light was chosen by a proper orientation of polarizer and analyzer allowing one to investigate the SHG signal in four different polarization combinations (pp, ps, ss, sp). The level of the SHG signals varied between 12 and 100 counts/s depending on the geometry and polarization combination. The maximum value was observed for pp combination of polarizations. The dark count rate was always less than 1 count/s. While rotating the polarizer the intensity of the excited light was kept constant (with an uncertainty of less than 5%) by means of a quarter wave plate placed just before the polarizer. The sample was mounted on a motorized rotational stage providing azimuthal rotation around the surface normal with high precision. The field dependences of the linear longitudinal Kerr effect (MOKE) in the Fe/Cr/Fe structures were measured with the same pulsed Ti:sapphire laser at an angle of incidence of 35° for s polarization of the fundamental beam. A high sensitivity was achieved by using a differential photodetector and lock-in technique. The average power incident on the sample for the MOKE measurements was kept below 1.0 mW in order to avoid saturation of the detector.

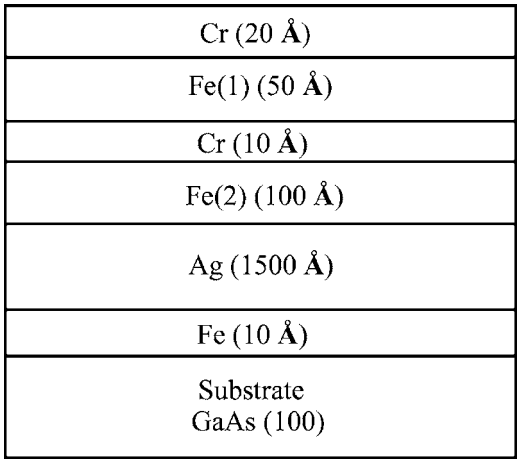

FIG. 2. Schematical layer sequence of the Fe/Cr/Fe samples investigated.

For comparison with the Fe/Cr/Fe structures the field dependences of MSHG and longitudinal MOKE were also measured on the Cr/Fe-wedge structures using the Ti:sapphire laser at $\lambda=800$ nm and a cw diode laser at $\lambda=670$ nm, respectively. The angle of incidence for these measurements was kept constant at about 10° for both methods.

The layer sequence of the Fe/Cr/Fe samples is schematically shown in Fig. 2. As a substrate material GaAs(100) wafers were used. The MBE growth was performed in a UHV chamber. To provide better epitaxy a thin (10 Å) Fe seed layer followed by a thick (1500 Å) Ag buffer layer were predeposited at 380 K on the *in situ* cleaned GaAs(100) surface and annealed for 1 h at 570 K.[57] After that the (100 Å) Fe(2) layer is grown. In order to prevent Ag segregation and simultaneously improve the interface quality, the substrate temperature was increased after the first 20 Å from room temperature to 480 K.[58] The (10 Å) Cr interlayer and the (50 Å) Fe(1) layer were deposited at room temperature. Finally, the entire stack was covered at room temperature by 20 Å of Cr to prevent oxidation. Typical growth rates for Fe and Cr were 0.1 Å/s. The Fe and Cr layers crystallized in the cubic bcc structure with (100) being the plane of growth. The crystal quality of the samples was controlled *in situ* by reflection high-energy electron diffraction (RHEED). Details of the growth procedure and an extensive characterization of Fe/Cr/Fe trilayers grown under these

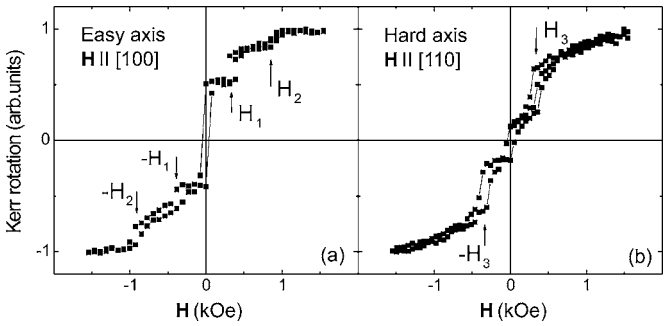

FIG. 3. Field dependences of the normalized longitudinal magneto-optical Kerr effect measured in a Fe(50 Å)/Cr(10 Å)/Fe(100 Å) sample with the magnetic field along easy (a) and hard (b) axes.

conditions can be found in Refs. 13 and 58. The Cr(20 Å)/Fe(x)/Ag(1500 Å)/Fe(10 Å)/GaAs(100) wedge structures with x varying from 100 to 500 Å along the [110] crystal axis (hard axis) were grown using the same recipe, except that the deposition rate of Fe was increased to 0.5 Å/s.

III. RESULTS

In Figs. 3(a) and 3(b) we present the magnetic field dependences of the normalized longitudinal MOKE signal measured in the Fe/Cr/Fe structure along the easy (**e**) and hard axes (**h**), corresponding to the [100] and [110] crystallographic directions in the plane of the sample, respectively. When the magnetic field is applied along the easy axis the Kerr rotation is characterized by strong jumps at $H=0$ and weaker jumps at $H_1=\pm 0.35$ kOe and $H_2=\pm 0.90$ kOe. At $H=0$ the bulk magnetizations $\mathbf{M}_1$ and $\mathbf{M}_2$ are oriented antiparallel along the easy axis, because the thickness of the Cr interlayer $t_{Cr}=10$ Å yields antiferromagnetic coupling in the $J_1(d_{Cr})$ dependence.[13] Nevertheless, the total magnetization $\mathbf{M}=\mathbf{M}_1+\mathbf{M}_2$ of the structure is nonzero, because the thickness of the Fe(1) layer is only half of Fe(2). The penetration depth of the laser light in the MOKE experiment is such that it also picks up a sizable Kerr signal from the bottom Fe(2) layer. The jump at $H=0$ thus corresponds to a switching of $\mathbf{M}$ into the opposite direction, i.e., a simultaneous reversal of $\mathbf{M}_1$ and $\mathbf{M}_2$. The jumps at $H=\pm H_1$ are caused by transitions into a nearly orthogonal phase $\mathbf{M}_1 \perp \mathbf{M}_2$, whereas the jumps at $H=\pm H_2$ mark the transition into the saturated state $\mathbf{M}_1 \| \mathbf{M}_2 \| \mathbf{H}$. When the magnetic field is applied along the hard axis the field dependence shows jumps at $H=0$ and $H_3=\pm 0.32$kOe. In this case, the magnetic field is oriented under ±45° to the easy axes. The jump at $H=0$ might correspond either to the magnetization reversal $\mathbf{M} \rightarrow -\mathbf{M}$ or the change of the direction of $\mathbf{M}$ by 90°. In both cases, the M_x component of the total magnetization responsible for longitudinal Kerr effect changes sign. The jumps at $H=\pm H_3$ arise due to a transition into a nearly orthogonal state. The saturated state is finally achieved by a subsequent rotation of the magnetizations in a field $H_s \approx \pm 2.5$kOe. The various magnetic configurations—which we will call phases in the following—that the system passes through when the magnetic field is applied along easy and hard axes are schematically presented in Fig. 4.

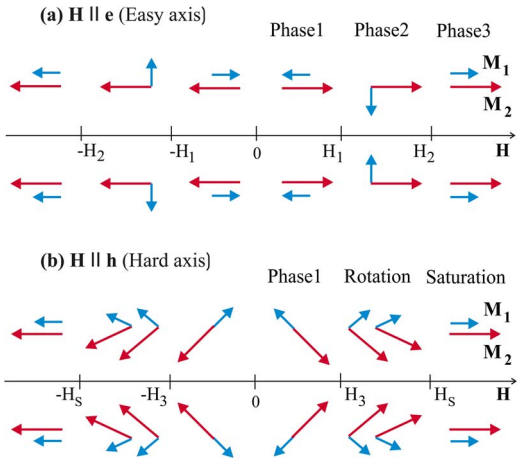

FIG. 4. (Color online) Various magnetic configurations arising during magnetization reversal with the field applied along easy (a) and hard (b) axis, respectively.

It has to be noted, that in both cases considered ($\mathbf{H} \| \mathbf{h}$ and $\mathbf{H} \| \mathbf{e}$) a magnetic domain structure can be formed, because magnetization states, which have a different sign of the magnetization component perpendicular to $\mathbf{H}$ are energetically equivalent. For $\mathbf{H} \| \mathbf{e}$ a domain structure may occur in the range of fields where an orthogonal phase exists. For $\mathbf{H} \| \mathbf{h}$, domains can exist in the entire range of fields $-H_s < H < H_s$, where H_s is the saturation field. For example, at $H=0$ the magnetization vectors in these domains are directed along the easy axes with the angle between them being 90°. Energetically equivalent states are shown in Fig. 4 above and below the field axes.

In Figs. 5 and 6 we show the dependence of the MSHG signal on the external field measured in the Fe/Cr/Fe structure for *pp* and *ss* combinations of the polarizations of the fundamental (ω) and the generated (2ω) light. The figures compile data for longitudinal and transversal geometries with the magnetic field applied along easy and hard axes. In all cases, we clearly observe significant changes in the SHG intensity level at the fields where transitions between different magnetic configurations ("phases") take place (compare to Figs. 3 and 4). The shape of these SHG variations depends essentially on both the experimental geometry (longitudinal or transversal) *and* on the combination of the polarization states. In contrast to the linear MOKE signal—which is an odd function of the magnetic field—the SHG field variations are even in *ss* and *ps* combinations of polarization states. In the *pp* and *sp* combinations, however, they do not possess a defined parity at all (*ps* and *sp* are not shown in Figs. 5 and 6). As a consequence, the jumps at $H=0$, which are clearly seen in linear MOKE do not appear in MSHG for certain polarization combinations. They are only seen for *pp* and *sp* polarizations in transversal geometry, when the magnetic field is applied along both easy and hard axes. When magnetizing along the easy axis ($\mathbf{H} \| \mathbf{e}$), the jumps at $H=\pm H_1$ are clearly seen for *pp* and *sp* in longitudinal geometry and for *pp*, *ss*, *ps*, *sp* polarization combinations in transversal geometry. The jumps at $H=\pm H_2$ are seen for *pp*, *ss*, *sp*, and *ps*

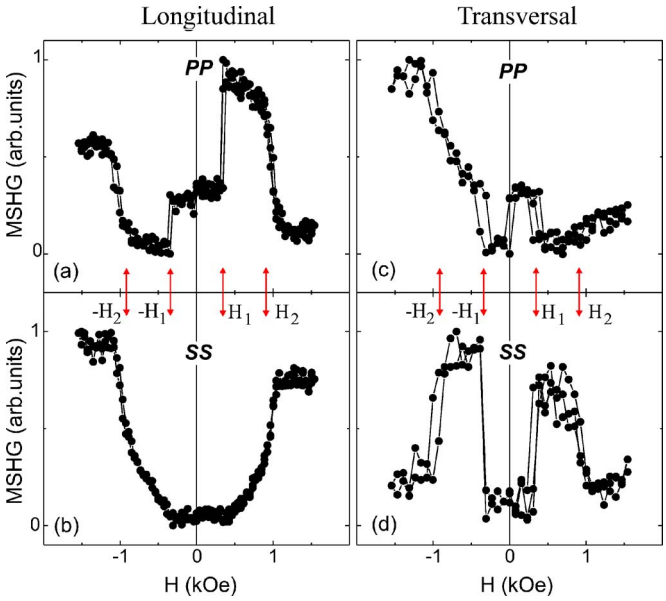

FIG. 5. (Color online) Field variations of the normalized MSHG signal measured of a Fe(50 Å)/Cr(10 Å)/Fe(100 Å) sample at magnetic field along the easy axis in longitudinal (a), (b) and transversal geometries (c), (d) for different combinations of light polarizations as indicated.

polarizations in longitudinal geometry and also observed for *pp* and *ss* polarizations in transversal geometry. Upon magnetizing along the hard axis ($\mathbf{H}\|\mathbf{h}$), the jumps in the SHG signal take place at $H=\pm H_3$ and appear both in the longitudinal and transversal geometries for *pp*, *ss*, *sp*, and *ps* polarizations. The count rate in longitudinal geometry for *pp* and *ss* polarization combinations was about 80 and 50 counts/s, respectively, and about 100 and 12 counts/s in transversal geometry.

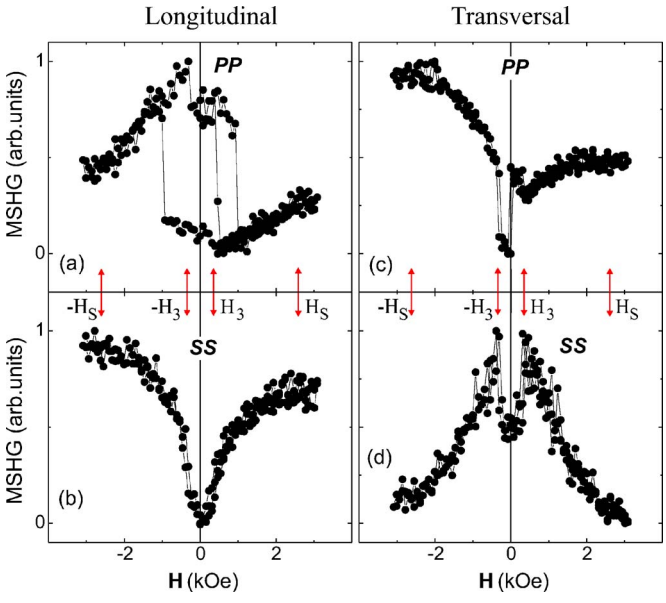

FIG. 6. (Color online) Field variations of the normalized MSHG signal measured of a Fe(50 Å)/Cr(10 Å)/Fe(100 Å) sample at magnetic field along the hard axis in longitudinal (a), (b) and transversal geometries (c), (d) for different combinations of light polarizations as indicated.

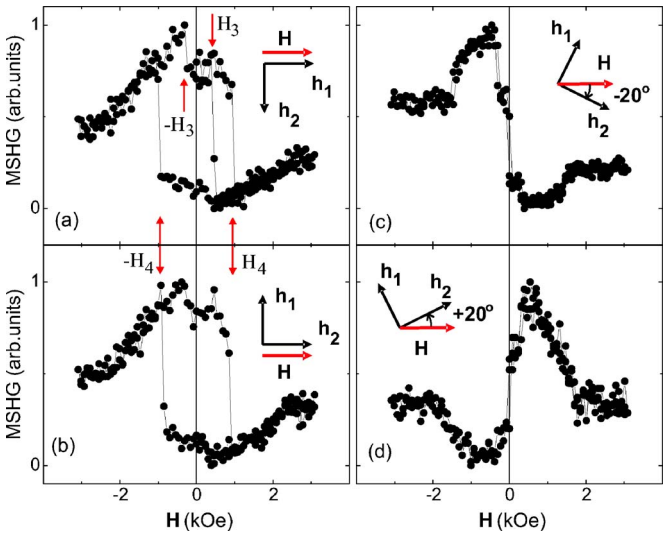

FIG. 7. (Color online) Field variations of the normalized MSHG signal measured of a Fe(50 Å)/Cr(10 Å)/Fe(100 Å) sample in longitudinal geometry for *pp* combination of light polarizations, when the magnetic field is applied along the two hard axes ($\mathbf{h}_1$ and $\mathbf{h}_2$), as well as at an angle of ±20° away from the hard axis $\mathbf{h}_2$.

One can see in Fig. 6(a) that the field dependence in longitudinal geometry for *pp* polarization principally differs from those measured in other polarizations and geometries, as well as from the Kerr effect. Only in this particular case the broad hysteresis with jumps taking place in the field range $H_s > |H_4| > H_3$ is observed. It should be noted that sometimes the jumps happen at the field values $\pm H_3$ corresponding to the transition into the orthogonal phase. In Fig. 7 we present the field variations in this geometry measured when the magnetic field is applied along both equivalent hard axes $\mathbf{h}_1$ and $\mathbf{h}_2$ of fourfold (biaxial) in-plane magnetic anisotropy, which are perpendicular to each other, as well as at an angle of ±20° away from one of the hard axes. We mention, that the shape of hysteresis depended on the position of the illuminated spot and, as it is seen in the Figs. 7(a) and 7(b), the jumps at the fields $H=\pm H_3$ can be accompanied by a partial or a complete change of magnetic state. A deviation of the magnetic field direction from the hard axis results in the disappearance of the broad hysteresis feature [Figs. 7(c) and 7(d)].

It has to be noted that the pulse energy density of fundamental beam used in our experiment is relatively small and we can neglect a possible demagnetization of the sample induced by the pump pulse, as is observed in time-resolved pump-probe experiments.[59,60] The following arguments additionally support this assumption. First, one should keep in mind that the SHG is a coherent process and generated on the time-scale of the pulse duration of ≈0.2 ps. The demagnetization happens with some delay defined by the spin-electron thermalization time, which is ≈0.1 ps. Thus, the maximal temperature of the spin subsystem is achieved just after the pulse termination. Secondly, we found that the MSHG and MOKE field dependences measured simultaneously in Fe/Cr/Fe and Cr/Fe-wedge structures can be

nicely described by the same values of magnetic energy potential (solid lines in Fig. 11). This clearly demonstrates that demagnetization does not play an important role in our measurements and can be neglected. Thirdly, we found experimentally that the shape of the field variations of the SHG did not change with an ≈25% intensity modulation of the fundamental beam.

IV. MODELING

In order to describe the field variations of the SHG signal in our experiments we employed a model considering the surface (air/Cr boundary), Cr/Fe(1), Fe(1)/Cr, Cr/Fe(2), Fe(2)/Ag interfaces as possible sources of electric-dipole SHG. As long as all layers crystallize in centrosymmetric structures, electric-dipole contributions from the bulk to SHG are absent. A volume contribution may arise due to quadrupole terms, but they are much smaller and we will neglect them in the following. The contributions to SHG from the interfaces below the thick Ag layer (d=1500 Å) are also negligible, because of the absorption in this layer. The nonmagnetic electric dipole contributions to SHG can arise from the surface as well as from interfaces. The magnetic contributions to SHG can only arise from Cr/Fe(1), Fe(1)/Cr, Cr/Fe(2), and Fe(2)/Ag interfaces. These contributions arise from 1 or 2 atomic layers at the interface and are related to interfacial magnetizations $\mathbf{m}_i$ of the Fe layers. We consider the value of the interfacial magnetization to be the same at all interfaces, although the volume magnetizations of the layers Fe(1) or Fe(2) are different, because of the asymmetry in the layer thicknesses. Therefore, we neglect interface induced moments in Cr and Ag as well as reduced or enhanced interfacial moments in Fe. We assume, that the symmetry of the surface and all interfaces is described by the C_{4v} symmetry group, since all layers are crystallized in a cubic bcc structure with a (100) surface orientation. For that symmetry the nonmagnetic contribution to SHG is described by a polar tensor χ^n_{ijk} of rank 3, which contains seven nonvanishing tensor components, with three of them being independent $\chi^n_{xzx}=\chi^n_{xxz}=\chi^n_{yzy}=\chi^n_{yyz}$, $\chi^n_{zxx}=\chi^n_{zyy}$, χ^n_{zzz}.[22] A magnetically induced contribution in longitudinal and transversal geometries is described by tensor χ^m_{ijk}, which contains ten independent nonvanishing components, whereby five of them are even and five odd under magnetization reversal. In longitudinal geometry the components odd in magnetization are χ^m_{yxx}, χ^m_{yyy}, χ^m_{yzz}, $\chi^m_{zyz}=\chi^m_{zzy}$, and $\chi^m_{xxy}=\chi^m_{yyx}$, but in transversal geometry these are χ^m_{xyy}, χ^m_{xxx}, χ^m_{xzz}, $\chi^m_{zxz}=\chi^m_{zzx}$, $\chi^m_{yyx}=\chi^m_{yxy}$. In the case of polar geometry the odd in magnetization components are $\chi^m_{xyz}=\chi^m_{xzy}=-\chi^m_{yxz}=-\chi^m_{yzx}$. The components even in magnetization coincide with the surface nonmagnetic ones in considered geometries. The intensity of the SHG light originates from an interference of the waves with frequency 2ω, generated at the surface and interfaces. Using the equations given in Refs. 55 and 56, taking into account a nearly normal incidence [$\sin(\theta)<<1$], and neglecting terms proportional to θ^2, as well as even in magnetization and linear in θ terms in the magnetic part of the nonlinear optical susceptibility appearing for *pp* and *sp* combinations of polarizations, it is straightforward to extract the contributions to SHG from one interface (or surface) for different polarization combinations, which are listed in Table I.

TABLE I. Contributions to SHG appearing in different combinations of the polarizations of the exciting and SHG light. Here χ^m_{ijk} and χ^n_{ijk} are linear on **m** and nonmagnetic nonlinear optical susceptibilities, respectively; N and n are refraction indices at 2ω and ω; θ is incidence angle and $\alpha_n=[2\chi^n_{xzx}/n+N\chi^n_{zxx}]$.

	m_x	m_y	m_z	nonmagnetic
$P_{\text{in}}P_{\text{out}}$	0	χ^m_{xxx}	0	$\alpha_n\theta$
$P_{\text{in}}S_{\text{out}}$	χ^m_{yxx}	0	$-\chi^m_{xyz}2\theta/n$	0
$S_{\text{in}}P_{\text{out}}$	0	χ^m_{xyy}	0	$N\theta\chi^n_{zxx}$
$S_{\text{in}}S_{\text{out}}$	χ^m_{yyy}	0	0	0

In our consideration the components of the tensor $\chi_{ijk}=\chi^n_{ijk}+\chi^m_{ijk}=\chi^n_{ijk}+\chi^m_{ijkl}m_l$ are defined in the physical coordinate system (Fig. 1). For isotropic films the crystallographic axes are not unambiguously defined in the plane of the film and can be chosen arbitrary. Therefore, the components of the tensor χ^n_{ijk} do not depend on rotation about the surface normal (z axis). Since for the C_{4V} symmetry the components of the tensor are the same as for the isotropic case, they do not change upon rotation as well. At the same time some components of the tensor χ^m_{ijkl} change upon rotation according to the rules[38] $\chi_{xxxx}=\frac{1}{4}\Delta\sin 4\varphi$, $\chi_{xxyx}=\chi'_{xxyx}-\frac{1}{2}\Delta\sin^2 2\varphi$, $\chi_{yxxx}=\chi'_{yxxx}-\frac{1}{2}\Delta\sin^2 2\varphi$, $\chi_{yyyx}=\chi'_{yyyx}+\frac{1}{2}\Delta\sin^2 2\varphi$, and $\Delta=\chi'_{yxxx}-\chi'_{yyyx}+2\chi'_{xxyx}$, where primed components refer to the crystallographic coordinate system and φ is the angle between the crystallographic [100] and x axes. We concentrate on the two most important cases, namely, when the magnetic field is applied along easy [100] (φ=0) and along hard [110] (φ=45°) axes. Obviously, in the latter case the transformation of the tensor components must be accounted for in calculations of the total SHG signal.

As it follows from the Table I the nonmagnetic SHG appears in *pp* and *sp* polarizations. The terms proportional to m_x appear in *ps* and *ss* polarizations, while the ones proportional to m_y show up in *pp* and *sp* polarization combinations. The structure of the tensor $\chi_{ijk}=\chi^n_{ijk}+\chi^m_{ijk}$ is the same for the surface and the different interfaces. Thus, in order to describe the magnetic contributions to SHG from the Fe(1) and Fe(2) layers it is convenient to use the effective nonlinear susceptibilities $\chi^{\text{eff},1}_{klm}$ and $\chi^{\text{eff},2}_{klm}$, which are associated with the interfacial magnetizations $\mathbf{m}_1$ and $\mathbf{m}_2$, correspondingly. However, introducing effective susceptibilities one should keep in mind that both "top" and "bottom" interfaces of each Fe(i) layer contribute to the effective susceptibilities $\chi^{\text{eff},i}_{klm}$. For example, for the Fe(1) layer, these are the Cr/Fe "top" and Fe/Cr "bottom" interfaces (see Fig. 2). Because in the ideal situation these interfaces are related by space inversion symmetry and the tensor describing the magnetic contributions to the SHG intensity is odd under this symmetry operation, the components $\chi^{i,\text{up}}_{klm}$ and $\chi^{i,\text{down}}_{klm}$ have the same value, but differ in sign. If we neglected the change of the intensity and phase of the exciting light at the "top" and "bottom" interfaces and the absorption of SHG in magnetic layer, the magnetic contributions to SHG from "top" and "bottom" interfaces would eliminate each other. However, the nonzero MSHG signals

TABLE II. Interfacial magnetization components in the different magnetic configurations with the magnetic field applied along the easy axis in longitudinal and transversal geometries. The upper and lower signs indicate positive and negative direction of the magnetic field, respectively.

	Longitudinal		Transversal	
	m_x	m_y	m_x	m_y
Phase I	$m_{1x}=\mp m$	$m_{1y}=0$	$m_{1x}=0$	$m_{1y}=\mp m$
	$m_{2x}=\pm m$	$m_{2y}=0$	$m_{2x}=0$	$m_{2y}=\pm m$
Phase II	$m_{1x}=0$	$m_{1y}=\pm m$	$m_{1x}=\mp m$	$m_{1y}=0$
	$m_{2x}=\pm m$	$m_{2y}=0$	$m_{2x}=0$	$m_{2y}=\pm m$
Phase III	$m_{1x}=\pm m$	$m_{1y}=0$	$m_{1x}=0$	$m_{1y}=\pm m$
	$m_{2x}=\pm m$	$m_{2y}=0$	$m_{2x}=0$	$m_{2y}=\pm m$

show the importance of these intensity and phase differences from the two interfaces. Note that the SHG intensity from the bottom Fe(2) layer is smaller than from the top Fe(1) layer, because of the absorption of light on the way to the surface. Therefore, we assume that the abovementioned changes of the phase and intensity and also possible nonequivalence of top Cr/Fe and bottom Fe/Cr interfaces (see Sec. V for the discussion of model limitations) are already included in the effective susceptibilities. Thus, the intensity of the SHG signal can be written in the form

$$I^{2\omega}_{\alpha\beta}=A|r^1_{\alpha\beta\gamma}m_{1\gamma}+r^2_{\alpha\beta\gamma}m_{2\gamma}+r_{\alpha\beta}|^2, \quad (1)$$

where A is a parameter depending on the intensity of the fundamental light, α and β are indices meaning s or p depending on the light polarization, and $\gamma=x,y,z$. The quantities $r_{\alpha\beta}$, $r^1_{\alpha\beta\gamma}$ and $r^2_{\alpha\beta\gamma}$ are defined by the components of the effective nonlinear susceptibilities $\chi^{\mathrm{eff},1}_{klm}$ and $\chi^{\mathrm{eff},2}_{klm}$, the structure of which is shown in Table I. For example, $r^1_{ppy}=\chi^{\mathrm{eff},1}_{xxx}$ etc. All parameters $r_{\alpha\beta}$, $r^1_{\alpha\beta\gamma}$, and $r^2_{\alpha\beta\gamma}$ are complex. As follows from Eq. (1) the contributions to the SHG signal linearly dependent on the magnetization arise from an interference between magnetic and nonmagnetic terms. Using Eq. (1) and setting the magnetization components of $\mathbf{m}_1$ and $\mathbf{m}_2$ according to the field-dependent magnetization phases (Fig. 4) in the longitudinal and transversal geometries, we simulated the field dependences of SHG for easy and hard axes.

A. Magnetic field along easy axis

When magnetized along the easy axis the changes of the magnetic structure may be approximately (neglecting magnetization rotation processes) represented in the form of transitions between collinear antiferromagnetic, orthogonal, and ferromagnetic phases [Fig. 4(a)]. The changes of the interfacial magnetization components in longitudinal and transversal geometries for a magnetic field directed along the easy axis are compiled in Table II. The SHG intensity described by Eq. (1) may contain linear and quadratic terms in $\mathbf{m}$ as well as nonmagnetic contributions. Terms quadratic in $\mathbf{m}$ and nonmagnetic contributions do *not* change upon magnetization reversal and their sum I_{mid} is the same for $+H$ and $-H$. In contrast, the sign of the contributions linear in $\mathbf{m}$ (called $\Delta I/2$) charges under magnetization reversal and is different for $+H$ and $-H$. Both I_{mid} and $\Delta I/2$ depend on the mutual orientation of the layer magnetizations $\mathbf{m}_1$ and $\mathbf{m}_2$ and differ in the various magnetic phases I to III. In Table III the expressions for these contributions in longitudinal and transversal geometries obtained through Eq. (1), Table I and Table II are presented.

In Fig. 8 the simulated field dependences of the MSHG response for *pp* and *ss* polarization combinations in longitudinal and transversal geometries at $\mathbf{H}\|\mathbf{e}$ are displayed. The

TABLE III. Intensity of the SHG signal in the different magnetic phases upon magnetizing along the easy axis for *pp* and *ss* configurations of polarization. Here I_{mid} is the part of the SHG response, which does not change sign under $\mathbf{H}$ reversal and $\Delta I/2$ is the SHG contribution changing sign under $\pm\mathbf{H}$ reversal. $\delta_1-\delta_5$ denote phase shifts between corresponding susceptibilities, and A is a coefficient proportional to I^2_ω.

	pp longitudinal	*pp* transversal
Phase I	$I_{\mathrm{mid}}=A\|r_{pp}\|^2$	$I_{\mathrm{mid}}=A[\|r_{pp}\|^2+\|(r^2_{ppy}-r^1_{ppy})m\|^2]$
	$\Delta I/2=0$	$\Delta I/2=\pm 2A\|r_{pp}\|\|(r^2_{ppy}-r^1_{ppy})m\|\cos\delta_1$
Phase II	$I_{\mathrm{mid}}=A(\|r_{pp}\|^2+\|r^1_{ppy}m\|^2)$	$I_{\mathrm{mid}}=A(\|r_{pp}\|^2+\|r^2_{ppy}m\|^2)$
	$\Delta I/2=\pm 2A\|r_{pp}\|\|r^1_{ppy}m\|\cos\delta_2$	$\Delta I/2=\pm 2A\|r_{pp}\|\|r^2_{ppy}m\|\cos\delta_3$
Phase III	$I_{\mathrm{mid}}=A\|r_{pp}\|^2$	$I_{\mathrm{mid}}=A[\|r_{pp}\|^2+\|(r^2_{ppy}+r^1_{ppy})m\|^2]$
	$\Delta I/2=0$	$\Delta I/2=\pm 2A\|r_{pp}\|\|(r^2_{ppy}+r^1_{ppy})m\|\cos\delta_4$
	ss longitudinal	*ss* transversal
Phase I	$I_{\mathrm{mid}}=A(\|r^1_{ssx}m\|^2+\|r^2_{ssx}m\|^2-2\|r^1_{ssx}m\|\|r^2_{ssx}m\|\cos\delta_5)$	$I_{\mathrm{mid}}=0$
	$\Delta I/2=0$	$\Delta I/2=0$
Phase II	$I_{\mathrm{mid}}=A\|r^2_{ssx}m\|^2$	$I_{\mathrm{mid}}=A\|r^1_{ssx}m\|^2$
	$\Delta I/2=0$	$\Delta I/2=0$
Phase III	$I_{\mathrm{mid}}=A(\|r^1_{ssx}m\|^2+\|r^2_{ssx}m\|^2+2\|r^1_{ssx}m\|\|r^2_{ssx}m\|\cos\delta_5)$	$I_{\mathrm{mid}}=0$
	$\Delta I/2=0$	$\Delta I/2=0$

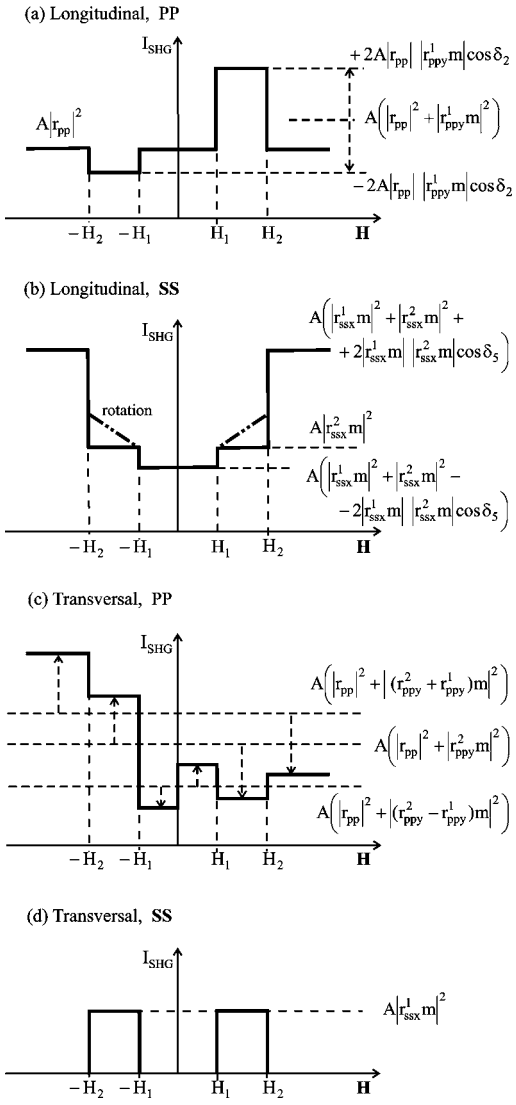

FIG. 8. Simulated field variations of the MSHG signal in longitudinal and transversal geometries at magnetic field along the easy axis ($\mathbf{H}\|\mathbf{e}$) for different polarization combinations.

values of the parameters $r^1_{\alpha\beta\gamma}$, $r^2_{\alpha\beta\gamma}$, and $r_{\alpha\beta}$ have been chosen such as to obtain a qualitative agreement of experimental and calculated curves. As one can see in Fig. 8 in accordance with the experimental curves (Fig. 5) the MSHG is an even function of the magnetic field in *ss* polarization combination, whereas the *pp* polarization field dependences do not exhibit a defined parity. The reversal of $\mathbf{m}_1$ and $\mathbf{m}_2$ at $H\approx 0$ does not manifest itself in longitudinal geometry in *pp*, and is also absent for both geometries in the *ss* signal. The result for the *pp* configuration is due to the fact that the component m_x does not contribute to MSHG in longitudinal geometry. For the *ss* configuration in longitudinal and transversal geometries the interference with the nonmagnetic SHG contribution is absent and in the transversal geometry in the regions $|H|<H_1$ and $|H|>H_2$ the magnetic contribution to SHG is absent. These features are also present in the experimental field variations (Fig. 5). The absence of the jump at $H=\pm H_1$ at *ss* polarization in longitudinal geometry shows that the values of $A(|r^1_{ssx}m|^2+|r^2_{ssx}m|^2-2|r^1_{ssx}m\|r^2_{ssx}m|\cos\delta_5)$ and $A|r^2_{ssx}m|^2$ are close, because the difference between them defines the magnitude of the jump. The observed strong increase of SHG in the experiment in the region $H_1<|H|<H_2$ is obviously associated with a rotation of the magnetization $\mathbf{m}_1$, i.e., a continuous field-induced change of the m_{1x} component. Using the approximate equality of the parameters mentioned above we can derive the expression for the SHG response in this field region

$$I^{2\omega}=A[|r^2_{ssx}m|^2+|r^1_{ssx}|^2(m^2_{1x}+m_{1x}m)], \tag{2}$$

where m_{1x} depends on the magnetic field as $m_{1x}=m\sin(\psi)$, with ψ being the angle between $\mathbf{m}$ and x axis, $\sin(\psi)\approx\xi H$, and ξ being defined by the magnetic anisotropy and exchange parameters. The relation between the parameters $|r^1_{ssx}m|^2$ and $|r^1_{ssx}m|^2+2|r^2_{ssx}m|^2$ is defined from the values of SHG at $H=0$ and at $H>H_2$ [see Fig. 5(b)]. That offers a chance to extract the azimuthal angle (ψ) of the magnetization $\mathbf{m}_1$ as a function of the field. For example, at $H=H_2$, $\psi=43°$. Note, that in the magnetization curves in the longitudinal MOKE the rotation of the magnetization shows up less pronounced, because in this case the rotation of the polarization plane measured in the experiment is associated with components of both bulk layer magnetizations M_{1x} and M_{2x}. The fact that in the longitudinal geometry in *pp* polarization the jumps at $H=+H_1$ and $H=-H_1$ (as well as at $H=+H_2$ and $H=-H_2$) have different signs shows that the rotation of magnetization $\mathbf{m}_1$ in the field $H=+H_1$ and $H=-H_1$ occurs into different directions, i.e., at $H=\pm H_1$, $\psi=\pm 90°$. Note, that the direction of magnetization rotation $\mathbf{m}_1$ for the magnetic field oriented along the easy axis is not defined by the strength of bilinear or biquadratic coupling or magnetic anisotropy. When accounting only for these interactions the states with $\psi=\pm 90^{\circ}$ are equally likely. The stabilization of one of these states might be associated with a small deviation of the magnetic field from the easy axis. In our experiments the misalignment of the field with the easy axis was less than 3°. It turns out that this misalignment was sufficient for realizing a monodomain structure over the whole field range.

In the transversal geometry in *ss* polarization the SHG signal in our model is related to the appearance of a m_{1x} component in the range of $H_1<|H|<H_2$. The field dependence of the SHG is symmetrical and shows two peaks in the field ranges $(-H_2,-H_1)$ and (H_1,H_2) [Fig. 8(d)]. In Fig. 5(d) these two peaks appear along with the weak background of the field-independent SHG. The origin of the background might be associated with the presence of the structural defects or quadrupole contributions to the SHG. The changes of the SHG in this and the longitudinal geometry are defined by changes of the $m_{1x}=m\sin(\psi)$ component.

The analysis of the field dependences of the SHG for different polarization combinations and geometrical configurations allows us to extract a relation between the different components of the nonlinear susceptibilities, e.g., $|r^2_{ppy}|/|r^1_{ppy}|\approx 0.7$, $|r^1_{ppy}|/|r_{pp}|\approx 0.5$, $|r^{1(2)}_{psx}/|r^{1(2)}_{ppy}|\approx|r^{1(2)}_{spy}/|r^{1(2)}_{ppy}|\approx 0.1$. Even at angles close to normal incidence ($\approx 5°$) the value of the nonmagnetic nonlinear susceptibility r_{pp} appears to be two times larger than the magnetic

TABLE IV. Intensity of the SHG signal of the various magnetic phases for magnetization reversal along the hard axis for *pp* and *ss* configurations of polarization. I_{mid} is the SHG contribution, which does not change sign under **H** reversal and $\Delta I/2$ is the SHG contribution changing sign under $\pm\mathbf{H}$ reversal. δ_1, δ_4 denote phase shifts between corresponding susceptibilities; A is a coefficient proportional to I_ω^2.

	pp longitudinal	*pp* transversal
$H=\pm 0$	$I_{\mathrm{mid}}=A(\lvert r_{pp}\rvert^2+\lvert(r^2_{ppy}-r^1_{ppy})m\rvert^2/2)$ $\Delta I/2=\pm\sqrt{2}A\lvert r_{pp}\rvert\lvert(r^2_{ppy}-r^1_{ppy})m\rvert\cos\delta_1$	$I_{\mathrm{mid}}=A(\lvert r_{pp}\rvert^2+\lvert(r^2_{ppy}-r^1_{ppy})m\rvert^2/2)$ $\Delta I/2=\pm\sqrt{2}A\lvert r_{pp}\rvert\lvert(r^2_{ppy}-r^1_{ppy})m\rvert\cos\delta_1$
$H=\pm H_3$	$I_{\mathrm{mid}}=A(\lvert r_{pp}\rvert^2+\lvert(r^2_{ppy}-r^1_{ppy})m\rvert^2/2)$ $\Delta I/2=\pm\sqrt{2}A\lvert r_{pp}\rvert\lvert(r^2_{ppy}-r^1_{ppy})m\rvert\cos\delta_1$	$I_{\mathrm{mid}}=A(\lvert r_{pp}\rvert^2+\lvert(r^2_{ppy}+r^1_{ppy})m\rvert^2/2)$ $\Delta I/2=\pm\sqrt{2}A\lvert r_{pp}\rvert\lvert(r^2_{ppy}+r^1_{ppy})m\rvert\cos\delta_4$
Saturation	$I_{\mathrm{mid}}=A\lvert r_{pp}\rvert^2$ $\Delta I/2=0$	$I_{\mathrm{mid}}=A(\lvert r_{pp}\rvert^2+\lvert(r^2_{ppy}-r^1_{ppy})m\rvert^2)$ $\Delta I/2=\pm 2A\lvert r_{pp}\rvert\lvert(r^2_{ppy}-r^1_{ppy})m\rvert\cos\delta_1$
	ss longitudinal	*ss* transversal
$H=\pm 0$	$I_{\mathrm{mid}}=A\lvert(r^2_{ssx}-r^1_{ssx})m\rvert^2/2$ $\Delta I/2=0$	$I_{\mathrm{mid}}=A\lvert(r^2_{ssx}-r^1_{ssx})m\rvert^2/2$ $\Delta I/2=0$
$H=\pm H_3$	$I_{\mathrm{mid}}=A\lvert(r^2_{ssx}+r^1_{ssx})m\rvert^2/2$ $\Delta I/2=0$	$I_{\mathrm{mid}}=A\lvert(r^2_{ssx}-r^1_{ssx})m\rvert^2/2$ $\Delta I/2=0$
Saturation	$I_{\mathrm{mid}}=A\lvert(r^2_{ssx}+r^1_{ssx})m\rvert^2$ $\Delta I/2=0$	$I_{\mathrm{mid}}=0$ $\Delta I/2=0$

one. The value r^1_{ppy} is larger than r^2_{ppy}. This finding can be associated with the fact that the Fe(1) layer is placed closer to the surface of the structure than Fe(2). The absorption of light generated at the interfaces of the Fe(2) film within the Fe(1) film decreases the value of r^2_{ppy} compared to r^1_{ppy}. The values of the $r^{1(2)}_{psx}$ and $r^{1(2)}_{spy}$ components determining the value of SHG in *ps* and *sp* polarization combinations are found to be one order of magnitude smaller than $r^{1(2)}_{ppy}$, which is a specific feature of transition metals.[61]

B. Magnetization reversal along hard axis

When the field is applied along the hard axis, in principle, several equivalent magnetic states may exist, because in this case there are two easy axis in each magnetic layer, oriented under ±45° to the magnetic field direction. Consequently, the magnetic states characterized by the same components of $\mathbf{m}_1$ and $\mathbf{m}_2$ along the magnetic field and components perpendicular to the magnetic field of different sign have equal energies. Here we consider the situation of a monodomain structure, with magnetic states in the field $+H$ and $-H$ being transformed into each other by the time reversal operation ($\mathbf{m}_1\rightarrow-\mathbf{m}_1$, $\mathbf{m}_2\rightarrow-\mathbf{m}_2$). For modeling this situation it is sufficient to define the SHG in different phases realized in this geometry at (i) $H=0$ (antiferromagnetic $\mathbf{m}_1\uparrow\downarrow\mathbf{m}_2$, $\mathbf{m}\angle\mathbf{H}=45°$), (ii) $H=\pm H_3$ (nearly orthogonal, $\mathbf{m}_2\perp\mathbf{m}_1$, $\mathbf{m}_1\angle\mathbf{H}\approx\pm 45°$), and (iii) $H>H_s$ (saturation area, $\mathbf{m}_1\|\mathbf{m}_2\|\mathbf{H}$). The expressions for SHG for the case of ($\mathbf{H}\|\mathbf{h}$) are shown in Table IV.

The simulated field variations of the MSHG signal in Fe/Cr/Fe structures for different combinations of polarizations in longitudinal and transversal geometries are presented in Fig. 9. The same parameters $r^1_{\alpha\beta\gamma}$, $r^2_{\alpha\beta\gamma}$ and $r_{\alpha\beta}$ as in Fig. 5 have been used to simulate these field variations.

The comparison with experiment (Fig. 6) shows that our model satisfactory describes the characteristic field dependences of the SHG in *ss* polarization for longitudinal geometry and *pp* polarization for the transversal geometry. At the same time for the longitudinal geometry, however, we find significant discrepancies when comparing to the experimental results in *pp* polarization (see Figs. 6 and 7). The field variations of the SHG signal in this geometry principally differ from the MOKE and SHG response in other geometries and polarization configurations. The main discrepancy consists in the width of the hysteresis loop, which is at least one order of magnitude broader than in the other cases. The field values at which the strong jumps of the SHG signal are observed ($H_4=\pm 0.90$kOe) do not coincide with the respective values in the linear Kerr effect measurements [see Fig. 3(b)].

Since for *pp* polarization in longitudinal geometry the SHG changes are given by the m_{1y} and m_{2y} components of the interfacial magnetizations, we must conclude that the strong jumps of the MSHG observed at $\pm H_4$ are associated with changes of mainly these components. We therefore have to expand our set of possible magnetic configurations considered so far. Magnetic state transformations, which are compatible with the observed changes of MSHG are shown in Fig. 10.

As the magnetic field decreases from the saturation value the magnetizations $\mathbf{m}_1$ and $\mathbf{m}_2$ rotate towards each other and finally arrive in an orthogonal state. At $+H_3$ the jumplike transition from the orthogonal to the antiferromagnetic configuration takes place, with the direction of $\mathbf{m}_1$ being changed by 90°. At $H=0$ the orientation of the magnetization vectors change, with the sign of their x components reversing and the y components remaining unchanged. At the field $-H_3$ $\mathbf{m}_1$ rotates by 90° so that the projection of the total magnetization $\mathbf{M}=\mathbf{m}_1+\mathbf{m}_2$ on the field axis increases. In the field $-H_4$ the magnetic state of the trilayer changes by jumping into another state characterized by a sign reversal of the y components of $\mathbf{m}_1$ and $\mathbf{m}_2$. A further increase of the field

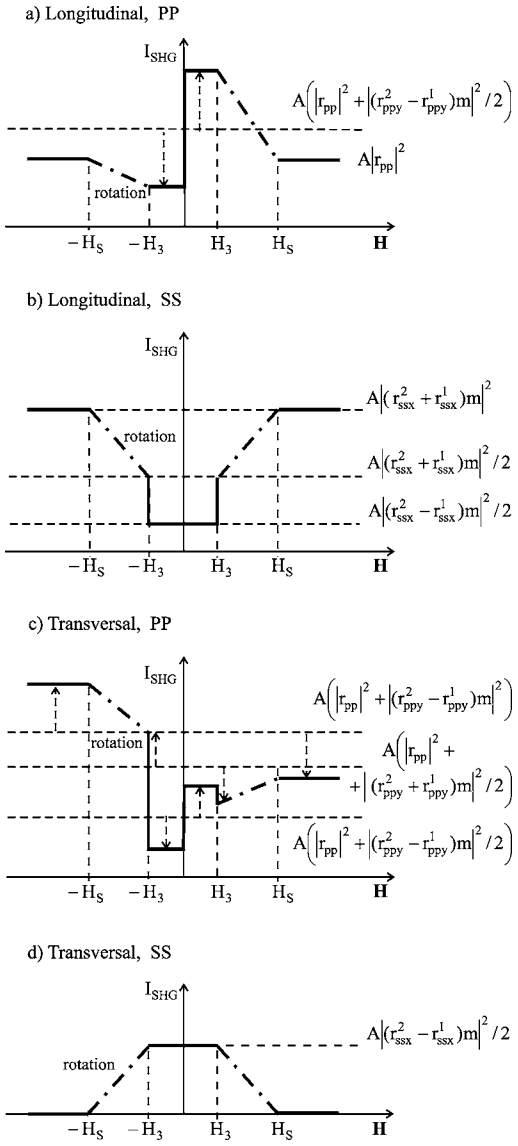

FIG. 9. Simulated field variations of the MSHG signal in longitudinal and transversal geometries at magnetic field along the hard axis ($\mathbf{H}\|\mathbf{h}$) for different polarization combinations.

brings the system into saturation by means of magnetization rotation. Going from saturation at $-H_s$ in the opposite direction to $+H_s$ the magnetic state transformations happen in a similar sequence.

Thus, jumps of the longitudinal x component in this geometry appear at $H=0$ and $H=\pm H_3$. They show up in the longitudinal MOKE loops, but do not manifest themselves in MSHG in the longitudinal geometry. The jumplike changes of the y components of $\mathbf{m}_1$ and $\mathbf{m}_2$ at $H=\pm H_4$, vice versa, can be discerned in MSHG, but do not appear in linear MOKE. The driving force for the transitions between two nominally degenerate states at $H=\pm H_4$ might be due to a symmetry-breaking mechanism, for example, the presence of a small nonzero H_y component caused by a minute deviation of the magnetic field from the hard axis. When this deviation becomes larger, however, the broad hysteresis in this geometry disappeared and only narrow loops were observed (Fig. 7). The experiment shows that the energy barrier between these nominally equivalent states is small and transitions between them could happen not only at the field H_4, but even at the smaller field $\pm H_3$, where the magnetic system switches into the orthogonal phase. It can be seen in Fig. 7(a) that at $H=-H_3$ the trilayer exhibits a partial and at $H=+H_3$ a full transition into the other state. The partial transition evidences that only in some part of the illuminated area on the sample the magnetic state transformation happened. Thus, the partial transformation is likely to be associated with the nucleation and growth of a new domain state by means of domain wall movement.

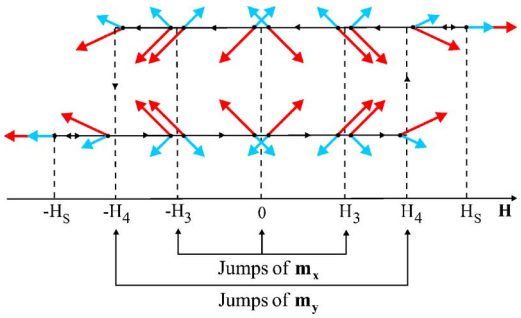

FIG. 10. (Color online) Magnetic state transformations resulting in the appearance of a broad hysteresis loop of the MSHG signal. Black arrows indicate the sequence of the field variation discussed in the text.

Upon magnetizing along the easy axis $\mathbf{H}\|\mathbf{e}$ in the longitudinal geometry in the *pp* polarization combination the broad hysteresis feature is absent. In this case, the change of the magnetic state in the region around $H=0$ happens between two monodomain states, with the sum magnetization $\mathbf{M}$ being parallel to the easy axis $\mathbf{e}$ and pointing into either one of the two directions. The system may switch to different energetically equivalent states only in the field regions where the canted phase is realized, $(-H_2,-H_1)$ and (H_1,H_2). In this situation, the presence of even a small angle between the direction of the magnetic field and the easy axis is enough to stabilize a monodomain state. In contrast to that, when applying the field along the hard axis $\mathbf{H}\|\mathbf{h}$, there is a probability of switching into different energetically equivalent states (see Fig. 4) already in the field regime close to $H=0$. The experiment shows that transitions happen so that only the sign of the m_x component changes, but the one of the m_y component remains unchanged. In this case, transitions between states of oppositely oriented m_y components are also possible, when $\mathbf{H}$ is not exactly parallel to $\mathbf{h}$.

Also in the transversal geometry in *pp* polarization the broad hysteresis feature in MSHG was not observed. In this case, in contrast to the longitudinal geometry, jumps of the m_y components of $\mathbf{m}_1$ and $\mathbf{m}_2$ are absent. For the *ss* polarization, in spite of the fact that the SHG arises from the m_x components, the jumps at $H=\pm H_4$ are also absent, because there is no interference with the nonmagnetic part of the SHG. In this case SHG intensity depends quadratically on the magnetization components and the field dependence is an even function.

With the aim to check the validity of the model of effective susceptibilities as well as to estimate the influence of the bottom interface on the susceptibility values in Fe/Cr/Fe

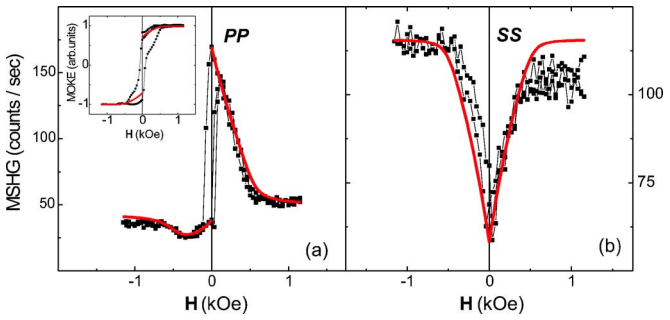

FIG. 11. (Color online) Field variations of the MSHG $[E_{ph}(2\omega)=3.1$ eV] signal measured for a Cr(20 Å)/Fe(x)-wedge sample at $x=490$ Å in longitudinal geometry for pp (a) and ss (b) polarization configurations at magnetic field along hard axis. The inset shows a MOKE measurement at $E_{ph}(\omega)=1.85$ eV. The red solid lines are simulations.

structures the field dependences of MSHG along with conventional MOKE were also measured on simpler Cr(20 Å)/Fe(x)-wedge structures containing only one Fe layer of variable thickness ($x=100-500$ Å). In Fig. 11 the field dependences of MSHG measured in such a structure for pp as well as ss polarization configurations are presented for $x=490$ Å and the magnetic field along a hard axis. The inset shows a conventional longitudinal MOKE measurement. The comparison of MOKE and MSHG field dependences in the case of a single Fe layer reveals that the changes of the magnetic state are associated with two processes. (i) The initial jump of the magnetization to opposite direction ($\mathbf{M}\rightarrow-\mathbf{M}$) near zero field. The magnetization in both phases before and after transformation is oriented along an easy axis. (ii) A subsequent rotation of the magnetization towards the external field when the field increases until saturation is achieved. Using Eq. (1) with $m_1=0$, the field dependences of MSHG can be calculated if the variation of the direction of $\mathbf{m}_2$ with magnetic field is known. The intensity of MSHG for the longitudinal geometry and pp combination of polarizations is given by $I=A|r'_{ppy}m\cos(\frac{\pi}{4}+\psi)+r_{pp}|^2$ and for ss combination of polarizations by $I=A|r'_{ssx}m\sin(\frac{\pi}{4}+\psi)|^2$, where ψ is the angle defining the equilibrium orientation of $\mathbf{m}_2$ relative to the nearest easy axis. The relations between parameters $r'_{ppy}m$, $r'_{ssx}m$, and $\cos(\delta)$ (where δ is phase shift between corresponding susceptibilities) are defined by the values of the MSHG intensity at field values, where the direction of the magnetization is known. These are the saturation area $I(H=\pm H_{sat})$, the points near the zero field $\Delta I/2(H\approx\pm 0)$, and the middle point at zero field $I_{mid}(H=0)$. The procedure of finding ψ is based on minimization of the magnetic energy potential W_m taking into account the biaxial in-plane magnetic anisotropy and the Zeeman energy, i.e.,

$$W_m=-\mathbf{MH}-\frac{K_1}{4}\cos^2(2\psi). \tag{3}$$

The magnetization value $M=1.71$ kG of bulk Fe and anisotropy constant $K_1=0.46\times10^6$ erg/cm^3 have been used to calculate ψ.[62] In Fig. 11 the calculated field dependences of MSHG are shown by solid lines and are found to be in good agreement with the experimental data for the following relations between for the effective susceptibilities $r'_{ppy}m/r_{pp}=1.8$, $r'_{ssy}m/r_{pp}=1.6$, $\cos(\delta_2)=0.64$. For the considered film of thickness $x=490$ Å the influence of the bottom Fe/Ag interface on the MSHG signal is practically absent because of the large absorption in the volume of the film. Therefore the extracted nonlinear susceptibilities characterize only the top Cr/Fe interface. As the thickness decreases below $x=150$ Å the shape of the field dependences and the values of the nonlinear susceptibilities remarkably change reflecting the contribution from the bottom Fe/Ag interface. In the inset of Fig. 11(a) the field dependence of the longitudinal MOKE calculated using the same parameters for the magnetic potential W_m as for the MSHG calculations are also shown. The fact that the field dependences of MSHG and MOKE can be described by the same magnetic potential, in particular, evidences that demagnetization processes induced by the light pulse practically do not appear in our measurements. We note that the magnetization rotation processes are significantly more pronounced in MSHG measurements in comparison with MOKE. In areas of Fig. 11, where the magnetization rotates, the MOKE signal is modified by about 30% of the maximal value, while for MSHG changes are $\approx$70 and $\approx$90 % for pp and ss polarization combinations, respectively.

V. LIMITATIONS OF THE MODEL APPROACH

Our model of a coupled magnetic structure taking into account the individual interfacial contributions to the MSHG gives in most cases a satisfactory qualitative description of the field dependences observed in different geometries and combinations of polarizations. Nevertheless, we also find distinct discrepancies between the model predictions and the experimental results, which should be noted. First of all, the model yet fails to explain the significant difference of the SHG intensities in longitudinal geometry and pp polarization for positive and negative fields in the saturation region ($|H|>H_s$), when $\mathbf{H}\|\mathbf{e}$ [Fig. 5(a)]. In addition, it does not account for the presence of jumps of the SHG signal in ss polarization, when magnetizing along the hard axis [Fig. 6(d)]. These shortcomings of the theory point out that the assumptions made in the model are probably still too simplified. The description can be improved, if linear in θ terms in the magnetic nonlinear optical susceptibility, which were neglected in our model, because of the smallness of θ, are taken into account. The linear in θ term proportional to m_z appearing in the ps combination of polarizations (see Table I) does not contribute to the SHG intensity, because the magnetization lies in the plane. However, the contribution proportional to m_x in the pp combination of polarizations might be responsible for the abovementioned difference visible in the SHG intensities in the saturation region for positive and negative fields. If so, one can conclude that the magnitude of χ^m_{xzx} and χ^m_{zxx} is at least one order of magnitude larger than the other components. The description might also be improved, if quadrupole contributions to the SHG intensity would also be included into our model.[63,64]

Two other mechanisms possibly giving rise to the discrepancies may be considered in the following. The first of them

is associated with the real symmetry of the interfaces. If the symmetry of at least one of the interfaces is lower than C_{4v}, in the tensor of the nonlinear susceptibility χ_{klm} new additional components will appear changing the relations between the individual SHG contributions and the magnetization components, which we have derived in Table I. In particular, additional terms may appear proportional to m_x components for the *pp* polarization and proportional to the y components of the interfacial magnetizations for the *ss* polarization. The contribution of such terms may lead to new features in the simulation, which are not described by the present model approach. However, the symmetry lowering of the interfaces is not likely. The anisotropy of the magnetic and optical properties, as well as the x-ray analysis of the trilayers clearly show the presence of a fourfold axis perpendicular to the plane of the substrate. Therefore, the possible symmetry lowering may only go from a point group C_{4v} to C_4. This is possible, if the crystallographic axis of the bottom layer does not coincide with the axis of the top one, but is rotated by a significant angle. In this case the symmetry element σ_v vanishes at the interface, but the C_4 axis is preserved. It seems that such a mechanism should be excluded, because it would be visible in the RHEED and LEED characterizations. It has to be noted, however, that microscopically the symmetry lowering might arise as a consequence of the interface being nonideal. The latter may arise due to interdiffusion of atoms of the neighboring layers or the presence of an atomic scale roughness at the interface. It is known, that about 0.1 ML of Fe diffuses into an Ag substrate.[3] The same is observed, when Cr is deposited on Fe. It is found that about 50% of the Cr atoms mix with Fe at a substrate temperature of 300 °C and the interface mixing is mostly confined to two atomic layers.[65–68] At the same time the interface alloying is an asymmetrical effect and it does not occur, when Fe is deposited on Cr as well as when Ag is deposited on Fe. Therefore, the Fe/Cr and Cr/Fe interfaces are not absolutely identical with respect to the stoichiometry. In the model considered this stoichiometric difference will show up as a difference of the absolute values of the tensors χ_{ijk}^{uo} and $\chi_{ijk}^{\mathrm{down}}$. However, because in our model we used only effective tensors $\chi_{ijk}^{\mathrm{eff}}$, we must point out that inclusion of this aspect will not change the results. The diffusion of atoms might result in the appearance of microscopical areas with lower symmetry at the interface. Nevertheless, if the distribution of the interdiffused atoms at the interface is random and does not display a certain order, the macroscopic symmetry remains an unchanged C_{4v}. Similar arguments may also be applied when considering the role of the interface roughnesses.

The second source, which could be responsible for the discrepancies of the model approach is associated with peculiarities of the interfacial magnetic structure. We assumed in our model that magnetic contributions in the nonlinear susceptibility arise only from the interfacial magnetizations of the Fe layers $\mathbf{m}_1$ and $\mathbf{m}_2$. In principle, the magnetic structure of the interface can be more complicated and may contain contributions of additional magnetic parameters characterizing the magnetic state of the intermediate layer, for example, a magnetization or antiferromagnetic moment of the Cr layer.[69] Several experimental and theoretical studies indicate that the first interfacial layer of Cr is in-plane ferromagnetically ordered and antiferromagnetically coupled to the Fe substrate.[52] In order to account in our model for the FM moment of Cr near the interface, it will be necessary to introduce additional nonlinear susceptibilities. For the case that the magnetic moments of Cr and Fe are strongly coupled and collinear, accounting for these susceptibilities leads only to a renormalization of the tensors $\chi_{ijk}^{\mathrm{eff}}$. The situation is principally different, however, if the magnetization of Cr aligns perpendicular to the Fe magnetization, e.g., due to frustrated magnetic nearest-neighbor interactions.[70] The presence of a perpendicular spin component in the Cr interlayer might, in principle, give rise to the abovementioned features of SHG in *pp* polarizations for $\mathbf{H}\|\mathbf{e}$ and *ss* polarizations at $\mathbf{H}\|\mathbf{h}$.

VI. CONCLUSIONS

Our investigations of magnetic second harmonic generation in exchange-coupled structures showed that this method is quite suitable to investigate in detail the various magnetic transitions occurring during a magnetization reversal cycle. It provides a means to separate the behavior of the individual components of the interfacial magnetizations $\mathbf{m}_1$ and $\mathbf{m}_2$. The study of the MSHG in certain combinations of polarizations and geometries allows one to follow the rotational processes of the interfacial magnetization contributions and the switching of their different components, when changing the magnetic state of the structure. As demonstrated, the MSHG approach is able to clearly resolve magnetic switching events in the trilayer, which may not be seen by traditional methods, e.g., by linear Kerr effect. In addition, as one can see from the comparison of field dependences of MSHG (Figs. 5 and 6) and MOKE (Fig. 3) the magnetization rotation processes are much more pronounced in the former. This, in principle, allows modeling of the magnetic thermodynamic potential more precisely and to define the parameters of magnetic anisotropy, bilinear and biquadratic interlayer exchange coupling with better accuracy than from the field dependences of linear MOKE alone. The main features of the MSHG field variations observed in the Fe/Cr/Fe structures are qualitatively described by the model, which suggests that the field-induced changes of the magnetic states at the interfaces take place in *grosso modo* analogously to that in the bulk of the films. At the same time some explicit distinctions are observed, giving evidence that the magnetic interface states nevertheless differ from the bulk ones. This brings up the point that in order to describe magnetic states of interfaces it is not sufficient to take into account only the layer magnetizations $\mathbf{M}_1$ and $\mathbf{M}_2$, but a careful consideration of the magnetic state of the interlayer and of the interfaces is also needed.

ACKNOWLEDGMENTS

The authors would like to thank O. A. Aktsipetrov for fruitful discussions and notices, and R. Schreiber for sample preparation. For B. B. Krichevtsov this work was partially supported by RFFI project (Grant No. 05-02-16451-a).

*Author to whom correspondence should be addressed. Electronic address: A.Rzhevsky@fz-juelich.de

[1] P. Grünberg, R. Schreiber, Y. Pang, M. B. Brodsky, and H. Sowers, Phys. Rev. Lett. **57**, 2442 (1986).
[2] D. E. Bürgler, P. Grünberg, S. O. Demokritov, and M. T. Johnson, in *Handbook of Magnetic Materials*, edited by K. H. J. Buschow (Elsevier Science, Amsterdam, 2001), Vol. 13.
[3] B. Heinrich and J. F. Cochran, Adv. Phys. **42**, 523 (1993).
[4] M. D. Stiles, J. Magn. Magn. Mater. **200**, 322 (1999).
[5] M. N. Baibich, J. M. Broto, A. Fert, F. Nguyen Van Dau, F. Petroff, P. Etienne, G. Creuzet, A. Friederich, and J. Chazelas, Phys. Rev. Lett. **61**, 2472 (1988).
[6] G. Binasch, P. Grünberg, F. Saurenbach, and W. Zinn, Phys. Rev. B **39**, 4828 (1989).
[7] D. M. Edwards, J. Mathon, R. B. Muniz, and M. S. Phan, Phys. Rev. Lett. **67**, 493 (1991).
[8] P. Bruno and C. Chappert, Phys. Rev. B **46**, 261 (1992).
[9] K. B. Hathaway, in *Ultrathin Magnetic Structures II*, edited by B. Heinrich and J. A. C. Bland (Springer-Verlag, Berlin, 1994).
[10] J. C. Slonczewski, Phys. Rev. Lett. **67**, 3172 (1991); J. Appl. Phys. **73**, 5957 (1993); J. Magn. Magn. Mater. **150**, 13 (1995).
[11] S. Demokritov, E. Tsymbal, P. Grünberg, W. Zinn, and Ivan K. Schuller, Phys. Rev. B **49**, 720 (1994).
[12] S. M. Rezende, C. Chesman, M. A. Lucena, M. C. de Moura, A. Azevedo, F. M. de Aguiar, and S. S. P. Parkin, J. Appl. Phys. **85**, 5892 (1999).
[13] C. M. Schmidt, D. E. Bürgler, D. M. Schaller, F. Meisinger, and H.-J. Güntherodt, Phys. Rev. B **60**, 4158 (1999).
[14] C. Carbone, E. Vescovo, O. Rader, W. Gudat, and W. Eberhardt, Phys. Rev. Lett. **71**, 2805 (1993).
[15] K. Garrison, Y. Chang, and P. D. Johnson, Phys. Rev. Lett. **71**, 2801 (1993).
[16] P. Segovia, E. G. Michel, and J. E. Ortega, Phys. Rev. Lett. **77**, 3455 (1996).
[17] T. P. A. Hase, I. Pape, D. E. Read, B. K. Tanner, H. Dürr, E. Dudzik, G. van der Laan, C. H. Marrows, and B. J. Hickey, Phys. Rev. B **61**, 15331 (2000).
[18] M. Hecker, H.-C. Mertins, D. Abramsohn, W. Gudat, and C. M. Schneider, J. Appl. Phys. **93**, 6516 (2003).
[19] M. Hecker, S. Valencia, P. M. Oppeneer, H.-C. Mertins, and C. M. Schneider, Phys. Rev. B **72**, 054437 (2005).
[20] N. N. Akhmediev, S. B. Borisov, A. K. Zvezdin, I. L. Lyubchanskii, and Yu. V. Melikhov, Sov. Phys. Solid State **27**, 650 (1985).
[21] Ru-Pin Pan and Y. R. Shen, Chin. J. Phys. (Taipei) **25**, 175 (1987).
[22] Ru-Pin Pan, H. D. Wei, and Y. R. Shen, Phys. Rev. B **39**, 1229 (1989).
[23] W. Hübner and K.-H. Bennemann, Phys. Rev. B **40**, 5973 (1989).
[24] O. A. Aktsipetrov, O. V. Braginskii, and D. A. Esikov, in *Proceedings of International Conference on Nonlinear Optics-13* (USSR, Minsk, 1988), Vol. 2, p. 142.
[25] O. A. Aktsipetrov, O. V. Braginskii, and D. A. Esikov, Sov. J. Quantum Electron. **20**, 259 (1990).
[26] J. Reif, J. C. Zink, C. M. Schneider, and J. Kirschner, Phys. Rev. Lett. **67**, 2878 (1991).
[27] M. Fiebig, D. Fröhlich, B. B. Krichevtsov, and R. V. Pisarev, Phys. Rev. Lett. **73**, 2127 (1994).
[28] A. Kirilyuk and Th. Rasing, J. Opt. Soc. Am. B **22**, 148 (2005).
[29] O. A. Aktsipetrov, T. V. Murzina, E. M. Kim, R. V. Kapra, A. A. Fedyanin, M. Inoue, A. F. Kravets, S. V. Kuznetsova, M. V. Ivanchenko, and V. G. Lifshits, J. Opt. Soc. Am. B **22**, 138 (2005).
[30] *Nonlinear Optics in Metals*, edited by K. H. Bennemann (Clarendon, Oxford, 1998).
[31] A. K. Zvezdin and V. A. Kotov, *Modern Magnetooptics and Magnetooptical Materials* (Institute of Physics, Bristol, 1997).
[32] L. C. Sampaio, J. Hamrle, V. V. Pavlov, J. Ferré, P. Georges, A. Brun, H. Le Gall, and J. Ben Youssef, J. Opt. Soc. Am. B **22**, 119 (2005).
[33] H. A. Wierenga, M. W. J. Prins, D. L. Abraham, and Th. Rasing, Phys. Rev. B **50**, 1282 (1994).
[34] H. A. Wierenga, W. de Jong, M. W. J. Prins, Th. Rasing, R. Vollmer, A. Kirilyuk, H. Schwabe, and J. Kirschner, Surf. Sci. **331**, 1294 (1995); Phys. Rev. Lett. **74**, 1462 (1995).
[35] H. A. Wierenga, M. W. J. Prins, and Th. Rasing, Physica B **204**, 281 (1995).
[36] T. A. Luce, W. Hübner, A. Kirilyuk, Th. Rasing, and K. H. Bennemann, Phys. Rev. B **57**, 7377 (1998).
[37] A. Kirilyuk, Th. Rasing, R. Megy, and P. Beauvillain, Phys. Rev. Lett. **77**, 4608 (1996).
[38] R. Atkinson and N. F. Kubrakov, Phys. Rev. B **65**, 014432 (2001); Appl. Phys. B **74**, 697 (2002).
[39] J. Hamrle, L. Polorecký, and J. Ferré, Phys. Rev. B **68**, 144401 (2003).
[40] A. Kirilyuk, J. Phys. D **35**, R189 (2002).
[41] L. C. Sampaio, J. Hamrle, A. Mougin, J. Ferré, F. Garcia, F. Fettar, B. Dieny, and A. Brun, Phys. Rev. B **70**, 104403 (2004).
[42] Y. Z. Wu, R. Vollmer, H. Regensburger, X.-F. Jin, and J. Kirschner, Phys. Rev. B **63**, 054401 (2000).
[43] L. C. Sampaio, A. Mougin, J. Ferré, P. Georges, A. Brun, H. Bernas, S. Poppe, T. Mewes, J. Fassbender, and B. Hillebrands, Europhys. Lett. **63**, 819 (2003).
[44] V. K. Valev, M. Gruyters, A. Kirilyuk, and Th. Rasing, Phys. Rev. Lett. **96**, 067206 (2006).
[45] V. K. Valev, M. Gruyters, A. Kirilyuk, and Th. Rasing, Phys. Rev. B **73**, 233101 (2006).
[46] S. O. Demokritov, A. B. Drovosekov, N. M. Kreines, H. Nembach, M. Rickart, and D. I. Kholin, JETP **95**, 1062 (2002).
[47] B. Heinrich, J. F. Cochran, T. Monchesky, and R. Urban, J. Appl. Phys. **87**, 5449 (2000).
[48] S. M. Rezende, C. Chesman, M. A. Lucena, A. Azevedo, F. M. de Aguiar, and S. S. P. Parkin, J. Appl. Phys. **84**, 958 (1998).
[49] A. Azevedo, C. Chesman, S. M. Rezende, F. M. de Aguiar, X. Bian, and S. S. P. Parkin, Phys. Rev. Lett. **76**, 4837 (1996).
[50] B. Heinrich, J. F. Cochran, T. Monchesky, and K. Myrtle, J. Appl. Phys. **81**, 4350 (1997).
[51] S.-H. Yang, B. S. Mun, N. Mannella, S.-K. Kim, J. B. Kortright, J. Underwood, F. Salmassi, E. Arenholz, A. Young, Z. Hussain, M. A. V. Hove, and C. S. Fadley, J. Phys.: Condens. Matter **14**, L407 (2002).
[52] H. Zabel, J. Phys.: Condens. Matter **11**, 9303 (1999).
[53] B. Koopmans, M. G. Koerkamp, Th. Rasing, and H. van den Berg, Phys. Rev. Lett. **74**, 3692 (1995).
[54] Th. Rasing, M. G. Koerkamp, B. Koopmans, and H. v. d. Berg, J. Appl. Phys. **79**, 6181 (1996).
[55] W. Hübner and K. H. Bennemann, Phys. Rev. B **52**, 13411 (1995).
[56] K. H. Bennemann, J. Magn. Magn. Mater. **200**, 679 (1999).
[57] D. E. Bürgler, C. M. Schmidt, J. A. Wolf, T. M. Schaub, and H.-J.

Güntherodt, Surf. Sci. **366**, 295 (1996).
[58] D. E. Bürgler, C. M. Schmidt, D. M. Schaller, F. Meisinger, R. Hofer, and H.-J. Güntherodt, Phys. Rev. B **56**, 4149 (1997).
[59] E. Beaurepaire, J.-C. Merle, A. Daunois, and J.-Y. Bigot, Phys. Rev. Lett. **76**, 4250 (1996).
[60] B. Koopmans, in *Spin Dynamics in Confined Magnetic Structures II*, edited by B. Hillebrands and K. Ounadjela, Vol. 87 of Topics in Applied Physics (Springer, Berlin, 2002), p. 253.
[61] W. Hübner, K. H. Bennemann, and K. Böhmer, Phys. Rev. B **50**, 17597 (1994).
[62] B. Heinrich and J. F. Cochran, Adv. Phys. **42**, 523 (1993).
[63] J. E. Sipe, D. J. Moss, and H. M. van Driel, Phys. Rev. B **35**, 1129 (1987).
[64] K. Sato, A. Kodama, M. Miyamoto, A. V. Petukhov, K. Takanashi, S. Mitani, H. Fujimori, A. Kirilyuk, and Th. Rasing, Phys. Rev. B **64**, 184427 (2001).
[65] R. Pfandzelter, T. Igel, and H. Winter, Phys. Rev. B **54**, 4496 (1996).
[66] J. F. Cochran, D. Venus, K. Totland, D. Atlan, S. Govorkov, and K. Myrtle, J. Appl. Phys. **79**, 4518 (1996).
[67] B. Heinrich, J. F. Cochran, D. Venus, K. Totland, C. M. Schneider, and K. Myrtle, J. Magn. Magn. Mater. **156**, 215 (1996).
[68] D. Venus and B. Heinrich, Phys. Rev. B **53**, R1733 (1996).
[69] V. N. Menshov and V. V. Tugushev, JETP **93**, 786 (2001); **95**, 901 (2002).
[70] D. Stoeffler and C. Cornea, Europhys. Lett. **56**, 282 (2001).